Water Practice & Technology

IWA PUBLISHING

Water Practice & Technology Vol 18 No 3, 592 doi: 10.2166/wpt.2023.023

Spatial evaluation of groundwater quality using factor analysis and geostatistical Kriging algorithm: a case study of Ibadan Metropolis, Nigeria

Emmanuel Oluwafemi Thomas

Department of Geography, University of Ibadan, Ibadan, Nigeria
E-mail: femiofficial8@outlook.com

EOT, 0000-0002-3506-5459

ABSTRACT

Necessity calls for the environmental aspects of groundwater to be evaluated and properly managed based on the observed spatial distribution with respect to quality, as it contributes to a significant portion of average water usage globally. Variations in groundwater quality in the Ibadan Metropolis might be a result of physical and chemical trends in the region leading to a decline in quality. The study was geared towards the spatial evaluation of groundwater quality using factor analysis and the Kriging algorithm. The parameters examined include pH, electrical conductivity, total dissolved solids, carbonates, chloride, nitrate, sulphate, calcium, sodium, magnesium, and potassium, which were sampled and analysed from the existing municipal deep wells in the Ibadan Metropolitan area; and distribution maps of each parameter were created using a geostatistical approach. Factor analysis examined the relationship between human activities and concentration levels. Semi-variograms were tested to ascertain the best-fitted model accuracy measures, average standard error, root mean square error, and root mean square error standardised. The groundwater index was calculated to ascertain the drinkability of the water in the study area. Overall, the result shows that the groundwater in the study area is suitable for consumption; drinking, and other uses. Kriging is a suitable assessment tool for modelling environmental parameters.

Key words: factor analysis, geo-statistics, groundwater, Kriging, water quality, water quality index

HIGHLIGHTS

- Geo-statistics was adopted to model the spatial distribution of concentration levels of parameters.
- Factor analysis was employed to elucidate the predominant lithological effect.
- The GWQI assessed groundwater suitability in the study area.
- Importance of geostatistical techniques in water quality modelling was presented.
- Importance of research to individuals and relevant agencies was presented.

GRAPHICAL ABSTRACT

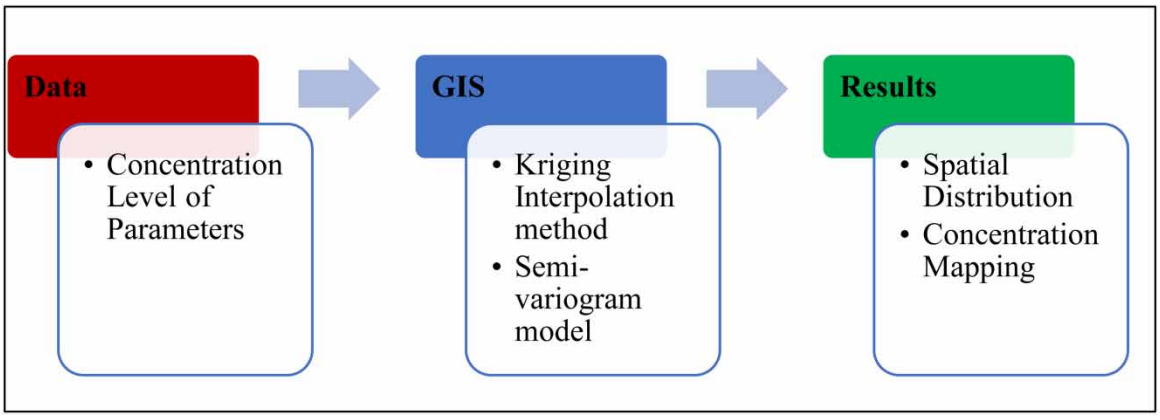

INTRODUCTION

Globally, the consumption of groundwater is to a large extent by a substantial portion of the world population, qualifying it as the most significant natural resource (Belkhiri *et al.* 2020). Groundwater contributes to roughly 95% of accessible freshwater globally and 31.5% of average water usage (Murphy *et al.* 2017). Groundwater is an important commodity, particularly in semi-arid and arid regions that constitute around 15% of the land surface of Earth, and is the sole resource available for people living in many arid and semi-arid regions (Díaz-Alcaide & Martínez-Santos 2019; Elubid *et al.* 2019). Groundwater has become an indispensable source of drinking water worldwide and especially in developing countries, becoming a primary water resource whose quality support is the prerequisite of groundwater usage, and is crucial to human health and social development (Xiao *et al.* 2018). The interaction between groundwater and the mineral content of the aquifer components through which it passes is largely responsible for variation in groundwater chemistry (Bouteraa *et al.* 2019). Variations in groundwater quality might be a result of physical and chemical trends in a region determined by anthropogenic activities, leading to a decline in quality (Elubid *et al.* 2019; Ali & Ahmad 2020).

In comparison to surface water, groundwater has unrivalled benefits in terms of spatiotemporal availability, high stability, simple accessibility, good quality, and contamination resilience (Murphy *et al.* 2017; Gu *et al.* 2018). Even though groundwater is not instantly tainted, it is difficult to eradicate pollutants once they have been introduced (Jiang *et al.* 2019; Wang *et al.* 2021). Geo-environmental concerns arise as a result of the continued extraction of groundwater resources and the socioeconomic disparities of urbanisation (He & Wu 2019). For sustainable development and successful groundwater management, it is vital to determine the mechanisms responsible for groundwater chemistry (Pazand *et al.* 2018; Aragaw & Gnanachandrasamy 2021). Rising population and rapid agricultural growth are the leading causes of aquifer overexploitation, which results in the degradation of groundwater quality (Aragaw & Gnanachandrasamy 2021), constant salinisation of topsoil, and decreased crop production (Boudibi *et al.* 2019).

Groundwater is branded by appallingly low-slung movement gradation, with an average domicile timeline of about 1,500 years in the aquifers (Saito *et al.* 2020). Throughout the extensive residence stretch, it consumes a reasonable time-spell to interconnect with the adjacent media of the aquifers (Thomas 2021), and damaging elements such as fluoride, arsenic, and additional lethal elements can turn out to be dissolved (Wang *et al.* 2018; Adimalla *et al.* 2019; Marghade *et al.* 2019). Additionally, numerous isolated constituents in groundwater have been portrayed to be higher in recent decades in different areas all over the world (Dar *et al.* 2017). For example, nitrogen (nitrates, nitrites, and ammonia) in aquifers have been revealed to be foremost in both metropolitan and rural districts. The origins of these multiplexes instigate divergences from inherent grounds, like outflows and septic pools, to agrarian actions (Busico *et al.* 2020). The gradation of the toxic component in groundwater has congruently been recognised in speedy upsurges in many locations, for instance, landfill spots, effluent/domesticated water irrigation lands, mining zones, and industrial situates (Ahmadi *et al.* 2018). The decline of water quality has been described in several aquifers globally (Jia *et al.* 2018; Dube *et al.* 2020).

Over the years, the concept of geostatistical interpolation and spatial correlation and respective applications have been reported by diverse array of researchers globally (Fallah *et al.* 2019). A number of researchers have applied the techniques of geospatial statistics in the examination of groundwater quality variation (Gharbia *et al.* 2016; Johnson *et al.* 2018; Belkhiri *et al.* 2020). Geo-statistics is a spatial statistical technique that can be used to assess and represent the distribution of concentration spatially and temporally (Narany *et al.* 2014). It predicts the estimated values based on the relationship between the sample points and estimates the uncertainty of that prediction. Kriging is a linear interpolation procedure that is used to create probabilistic models of uncertainty relating to the values of the attributes. Hence, when spatial information is mapped together, it creates a powerful means for monitoring and management (Ali & Ahmad 2020).

Recent advances in the use of the geographic information system (GIS) have expanded its capabilities for spatiotemporal data to establish the distribution pattern of water quality variables (Bouteraa *et al.* 2019), and to map groundwater quality evaluation using geo-statistics (Nas & Berktay 2010; Selmane *et al.* 2022). To map the spatial variability, geo-statistics uses Kriging, the best linear unbiased estimator for predicting missing data at unknown places, which is the most widely used approach for environmental studies, particularly in ecological and water quality investigations. Recent advances in the use of the GIS have expanded its capabilities for spatiotemporal data to establish the geographic range of groundwater quality parameters and to map groundwater quality evaluation using geo-statistics (Venkatramanan *et al.* 2016).

Groundwater quality science has advanced rapidly during the last three decades, and significant progress has been made (Li *et al.* 2019). Kriging is a well-known geostatistical interpolation approach that is based on the spatial connections between the various measures surrounding the forecast site (Obaid & Mohammed 2020). The approach is an estimating procedure that determines unknown values using known values and a variogram (Selmane *et al.* 2022). When estimating values at unknown positions, it considers both the distance and the degree of variance between known data positions (Rata *et al.* 2018).

MATERIALS AND METHODS

Study area description

Ibadan (the capital of Oyo State, Nigeria) is located in the heart of Southwest Nigeria, ranks third concerning the population after Lagos and Kano states, and with respect to the geographical area, it is the largest city in Nigeria (Figure 1). Ibadan has an alternating wet, of up to 8 months, and dry, of about 4 months, seasons with relatively constant atmospheric temperature per annum. The mean maximum temperature of Ibadan is about 26.46 °C, the mean minimum temperature of 21.42 °C, and relative humidity of 74.55% (Amanambu 2015). The month of June has the highest record of mean monthly rainfall of approximately 125 mm, with January having the lowest of approximately 18 mm. The mean annual rainfall is about 1,205 mm, which falls for about 109 days, having two peaks in June and September (Egbinola & Amanambu 2014).

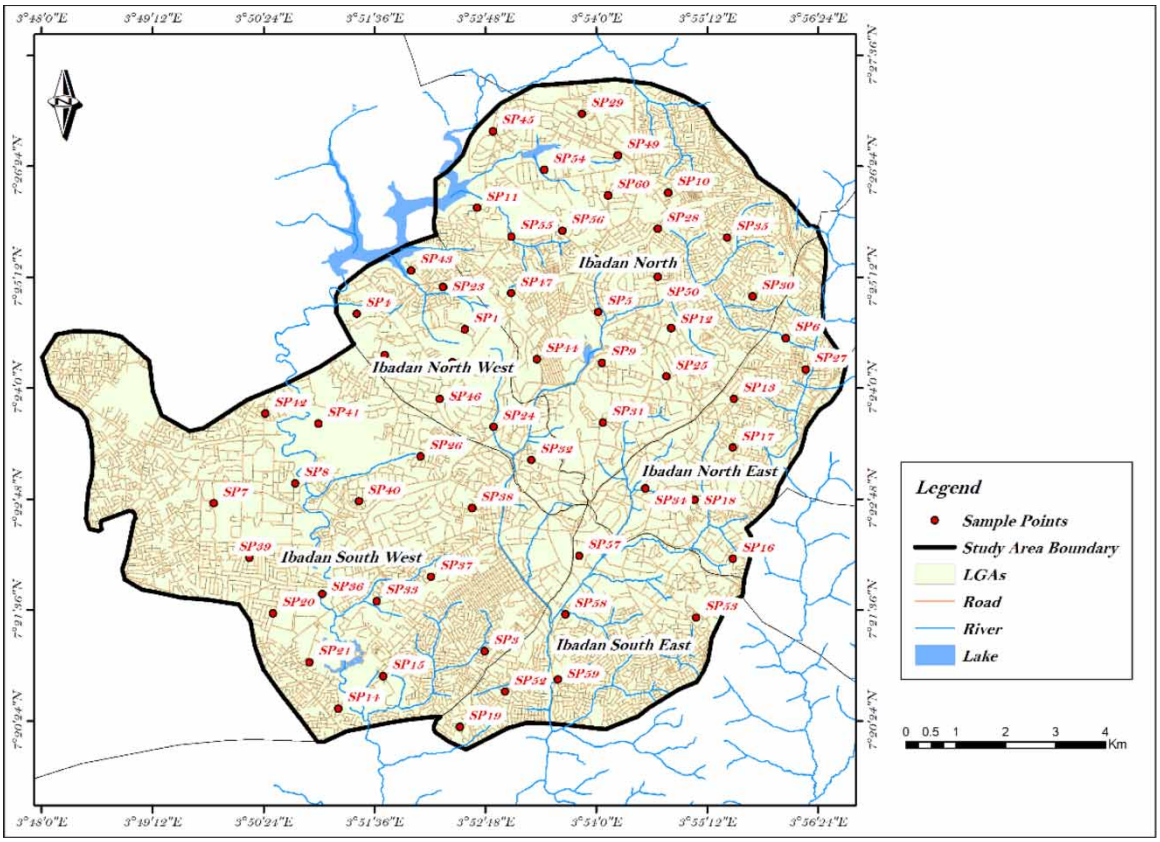

Figure 1 | Map showing the study area.

The study site is underlain by a basement complex, characterised by igneous and metamorphic rocks of the Precambrian era. Granite quartzite and migmatite are the major rock types (Egbinola & Amanambu 2014). Usually, the rock types found within this area are regarded as poor aquifers, given their low permeability and porosity (Egbinola & Amanambu 2014; Amanambu 2015). Though, some levels of porosity and permeability are developed through fractures and weathering, which in turn depends on the parent material. Therefore, the accessibility of groundwater depends on the weathered material's level and the extent to which joints and fractures are present (Egbinola & Amanambu 2014).

Methodology

To assess the level of groundwater contamination, sampling of groundwater is done from hand-dug well located in the study area's residential and agricultural areas. Good quality narrow mouth screw-capped polypropylene bottles of 2-l capacity were used to collect the sample. Bottles were first washed with dilute nitric acid, and then rinsed thrice with DM (demineralised) water. The groundwater samples retrieved in prewashed polyethylene bottles were analysed for the following parameters: pH, E.C., and TDS, and were taken onsite with the aid of a multi-parameter water meter. The concentrations of calcium (Ca^{+}) and magnesium (Mg^{+}) were measured by the volumetric method in the presence of an aqueous ethylenediamine tetraacetic acid (EDTA) solution; this method was also used for titration of carbonates (HCO_3). Chloride (Cl^{-}) was determined in the neutral medium by a titrated solution of silver nitrate in the presence of potassium chromate. The measurement of nitrates (NO_3^{-}) and sulphate (SO_4^{2-}) was carried out by a spectrophotometric method (Bashir *et al.* 2020), and potassium (K^{+}) and sodium (Na^{+}) measurements were determined by a flame photometer (Bouteraa *et al.* 2019).

RESULTS AND DISCUSSION

Groundwater hydrochemistry of the study area

A descriptive analysis was carried out on the data, as well as a test for normality with respect to the distribution of the data. The result of the analysis is given in Table 1; the mean pH value is 6.48 while the pH of the whole dataset ranges between 4.40 (minimum) and 7.10 (maximum), this shows that the water samples obtained lie within the permissible limit for natural and potable water, respectively. The range of electrical conductivity (E.C.) lies within 270 μS/cm (minimum) and 1,870 μS/cm (maximum), while the average E.C. is 893.38 μS/cm. The total dissolved solids (TDS) ranges between a minimum of 142 mg/l and a maximum of 1,720 mg/l, with a mean TDS of 667.88 mg/l. It is obvious that there is a strong affinity between the presence of high TDS and high values of E.C. The result of the data (Table 2) skewness analysis revealed that majority of the data sets of the parameters under consideration were positively skewed, however, some are more positively skewed than others. Noteworthy is the skewness of the parameters, 'pH, calcium, and sulphate' which are the negatively skewed parameters under consideration. In conclusion the dataset does not entirely appear to be normally distributed, however, these were normalised by employing the log-normal distribution during analysis.

Table 1 | Summary statistics of parameters

Parameter	N	Minimum	Maximum	Mean	Std. deviation	Skewness	
pH	60	4.40	7.10	6.4880	0.49104	−2.133	0.309
EC (μS/cm)	60	270.00	1,870.00	893.5585	326.55731	0.650	0.309
TDS (mg/l)	60	142.00	1,720.00	536.8767	290.22752	2.322	0.309
Sodium (mg/l)	60	5.10	59.52	31.9623	13.94075	0.151	0.309
Magnesium (mg/l)	60	3.73	9.50	6.0187	1.25199	0.496	0.309
Calcium (mg/l)	60	1.30	7.37	4.7102	1.33943	−0.618	0.309
Chloride (mg/l)	60	57.60	1,476.00	445.0062	304.69540	0.899	0.309
Potassium (mg/l)	60	0.00	6.10	2.2550	1.30636	0.763	0.309
Carbonate (mg/l)	60	100.50	609.00	253.0008	111.75046	1.116	0.309
Sulphates (mg/l)	60	0.22	35.13	19.6747	9.78644	−0.039	0.309
Nitrates (mg/l)	60	0.63	39.06	9.6590	7.43786	2.008	0.309

Hydrochemistry and anthropogenic activities

The analysed groundwater samples were subjected to factor analysis in order to acquire an overall idea about assembling the samples in a multidimensional space specified by the assessed parameters. Factor analysis is a valuable approach for gaining a better understanding of the connection between variables and identifying groupings (or clusters) that are mutually associated with a data body. The anthropogenic land use activities identified in the study area include educational, residential, commercial, waste disposal, and industrial activities, respectively. These land use activities gave rise to the prevalent factors identified affecting the quality of groundwater in the study area. These include use of pesticides, fertilisers, effluents and industrial wastes, landfills and waste

Table 2 | Concentration level of parameters

SS	pH	EC (μS/cm)	TDS (mg/l)	K^+ (mg/l)	Na^+ (mg/l)	Mg^{2+} (mg/l)	Ca^+ (mg/l)	Cl^- (mg/l)	HCO_3^- (mg/l)	SO_4^{2-} (mg/l)	NO_3^- (mg/l)
1	6.80	548.00	471.90	92.32	40.50	4.94	7.37	57.60	156.04	33.34	39.06
2	6.80	432.00	658.60	42.58	40.38	6.13	5.35	57.60	151.05	29.42	20.10
3	6.80	1,020.00	625.60	66.25	40.31	5.72	2.85	86.40	156.05	26.31	6.40
4	6.90	1,010.00	330.50	96.03	40.58	7.15	5.13	151.20	156.03	31.28	3.05
5	6.80	990.00	831.60	99.05	40.37	5.54	5.57	115.20	100.50	21.79	2.97
6	6.90	779.00	422.40	73.28	40.54	5.54	5.28	64.80	244.04	29.11	5.38
7	6.85	1,870.00	508.80	40.23	45.85	5.87	5.47	108.00	250.05	32.65	4.70
8	7.01	1,115.00	557.70	47.32	45.53	5.47	3.48	208.30	156.05	17.69	8.78
9	7.00	1,294.00	924.00	97.04	40.56	3.73	5.54	525.60	200.04	10.26	3.76
10	6.81	1,470.00	324.70	45.89	42.51	5.38	4.07	180.00	200.20	11.26	8.22
11	6.80	1,420.00	271.90	31.25	46.56	5.37	5.29	237.60	290.06	19.66	10.75
12	7.00	1,470.00	452.70	61.85	52.19	5.37	5.40	302.60	154.04	11.56	13.29
13	6.80	270.00	361.60	59.75	40.36	5.06	5.52	187.20	144.50	9.35	14.27
14	6.80	1,710.00	289.00	64.55	59.52	5.04	5.82	208.30	250.04	27.33	12.71
15	6.81	715.00	673.20	66.62	57.05	5.29	5.58	288.00	156.05	33.59	14.76
16	6.70	998.00	666.50	55.40	50.06	5.06	5.85	259.20	156.05	10.79	18.68
17	6.80	948.00	653.40	47.40	50.02	5.54	5.30	170.30	156.05	22.53	10.72
18	7.00	480.50	950.40	55.39	45.08	5.84	5.07	107.00	156.03	13.78	5.98
19	7.00	1,260.01	564.50	46.89	47.65	5.03	3.36	109.80	156.03	23.86	20.12
20	6.70	640.00	1,470.00	60.00	45.52	5.47	3.14	187.50	156.04	24.21	9.99
21	6.80	771.00	1,470.00	50.63	50.52	5.45	2.54	152.00	200.20	28.15	2.79
22	6.80	845.00	142.00	60.54	56.81	5.06	5.33	206.00	244.04	31.82	3.34
23	6.70	1,400.00	1,720.00	62.35	45.04	5.46	5.14	409.57	290.85	9.67	6.79
24	6.80	492.00	603.50	56.37	48.58	5.17	5.39	242.00	156.05	12.39	8.21
25	6.80	412.00	752.60	59.01	50.65	5.64	5.67	460.50	144.50	11.68	1.83
26	6.30	553.00	353.90	40.40	35.40	5.90	7.30	360.00	609.00	18.97	2.53
27	6.80	602.00	350.00	62.40	22.40	4.60	2.30	602.00	276.60	15.78	9.37
28	6.20	860.00	540.00	56.50	20.70	7.60	4.90	429.00	219.44	25.23	11.15
29	6.60	884.00	390.00	64.00	20.70	6.30	5.40	724.60	284.72	26.54	9.87
30	6.60	924.00	366.70	64.00	19.60	8.70	3.00	360.00	203.00	21.65	11.56
31	6.20	818.00	500.00	57.80	20.70	7.50	4.30	439.50	224.13	2.16	37.56
32	6.30	944.00	480.00	53.40	20.50	7.70	5.70	408.00	210.07	13.79	18.60
33	6.20	403.00	257.90	24.40	8.60	6.30	4.60	144.00	460.00	15.73	5.20
34	6.20	753.00	350.00	58.10	22.90	6.30	1.30	753.00	225.40	9.70	1.85
35	4.40	820.00	420.00	75.30	27.20	5.90	5.60	820.00	353.00	6.47	1.77
36	6.30	513.00	328.50	49.30	15.30	6.80	6.10	252.00	446.00	13.36	4.88
37	6.70	915.00	420.00	42.50	25.60	4.40	6.40	915.00	187.48	15.09	3.00
38	6.50	753.00	481.90	77.70	23.40	9.50	6.60	558.00	469.00	11.64	7.08
39	6.00	1,044.00	600.00	58.70	28.70	7.30	4.90	930.00	283.00	9.05	2.26
40	6.70	1,283.00	821.10	98.80	26.80	5.60	5.60	1,476.00	353.00	10.13	6.92
41	6.40	957.00	390.00	43.90	24.00	5.60	3.20	957.00	353.00	32.33	9.45
42	6.50	596.00	400.00	28.80	24.50	4.60	4.70	596.00	276.60	32.97	11.99
43	6.60	823.00	420.00	29.10	25.10	4.50	4.60	823.00	225.40	35.13	12.97
44	6.80	706.00	400.00	41.20	26.10	4.20	5.80	706.00	161.29	31.47	11.41
45	4.70	770.00	430.00	41.80	26.70	4.00	6.20	770.00	283.00	28.66	13.46

(*Continued.*)

Table 2 | Continued

SS	pH	EC (μS/cm)	TDS (mg/l)	K^+ (mg/l)	Na^+ (mg/l)	Mg^{2+} (mg/l)	Ca^+ (mg/l)	Cl^- (mg/l)	HCO_3^- (mg/l)	SO_4^{2-} (mg/l)	NO_3^- (mg/l)
46	6.30	883.00	309.10	26.20	9.40	7.10	2.90	306.00	340.00	33.62	17.38
47	6.30	1,083.00	693.10	91.20	26.10	7.50	2.50	1,062.00	426.00	20.69	11.82
48	6.20	9,64.00	379.50	29.30	10.80	7.90	5.10	486.00	113.00	27.80	7.08
49	6.10	1,004.00	328.30	41.90	13.30	6.80	3.40	600.00	147.00	35.13	21.22
50	7.10	813.00	520.30	64.10	17.80	4.30	4.90	828.00	283.00	26.94	11.09
51	6.30	611.00	320.00	56.10	23.40	4.30	2.10	611.00	283.00	5.39	1.69
52	5.90	1,084.00	450.00	50.70	25.70	7.40	2.30	910.00	353.00	0.22	3.82
53	6.30	902.00	550.00	56.10	20.60	7.60	2.30	418.50	214.76	5.17	5.29
54	5.80	1,123.00	400.00	55.20	24.80	7.50	5.70	712.00	163.51	29.96	10.11
55	6.00	513.00	328.30	9.80	5.10	6.40	4.80	558.00	423.00	15.52	3.73
56	6.10	673.00	430.70	63.90	18.40	5.80	4.40	576.00	501.00	4.96	.63
57	6.00	1,183.00	757.10	99.60	38.00	7.30	4.90	540.00	370.00	26.32	7.47
58	6.10	483.00	309.10	51.10	15.80	6.90	5.10	103.00	473.00	17.53	9.25
59	6.40	986.00	440.00	57.40	20.50	7.80	4.80	397.50	205.38	9.56	8.67
60	6.40	1,028.00	600.00	59.70	20.40	7.90	4.40	487.00	200.69	12.34	10.76

dumpsites, and septic discharge. These are associated with the dominant land use around each sample location. All samples were subjected to factor analysis, which revealed a 0.587 value for the Kaiser–Maiyer–Olkin (KMO) and a value of 241.159 (p 0.000) for Bartlett's sphericity, indicating that FA was effective in giving significant reductions in dimensionality. From the data, four factors (Table 3), explaining 98.35% of the total variance, were estimated on the basis of the Kaiser criterion (Kaiser 1960) of the eigenvalues greater than or equal to 1.

Table 3 | Rotated factor loading matrix showing eigen values of parameters

	Factor			
Parameters	**1**	**2**	**3**	**4**
pH	.024	−0.996	−0.017	−0.018
EC	.993	0.007	−0.051	−0.079
TDS	.749	−0.159	−0.609	0.163
Sodium	.848	0.148	−0.243	0.430
Magnesium	.798	−0.512	.314	0.020
Calcium	.117	0.810	.527	0.133
Chloride	.542	0.443	−0.108	−0.695
Potassium	−0.961	−0.058	0.242	0.053
Carbonates	−0.734	0.215	−0.469	0.440
Sulphates	.408	0.879	0.004	0.209
Nitrates	.570	−0.302	0.607	0.397
Total eigen value	5.167	3.067	1.469	1.117
% of variance	46.969	27.883	13.352	10.151
Cumulative %	46.969	74.852	88.205	98.356

A scree plot is a basic linear graph that illustrates the proportion of total variation explained or represented by each element in the data. The factors are arranged, and therefore given a number label, in decreasing order of contribution to the total variance. A scree plot is a graph of eigenvalues in ascending order of magnitude. It demonstrates a clear distinction between the slope angle of the strong eigenvalues and the progressive falling off of the remaining components. The four extracted components (eigenvalues > 1) appropriately represented

the aggregate dimensions of the data set and compensated for 98.356% of the total variance in the current research, whereas the other six factors (eigenvalues 1) accounted for just 1.644% of the total variance (Figure 2).

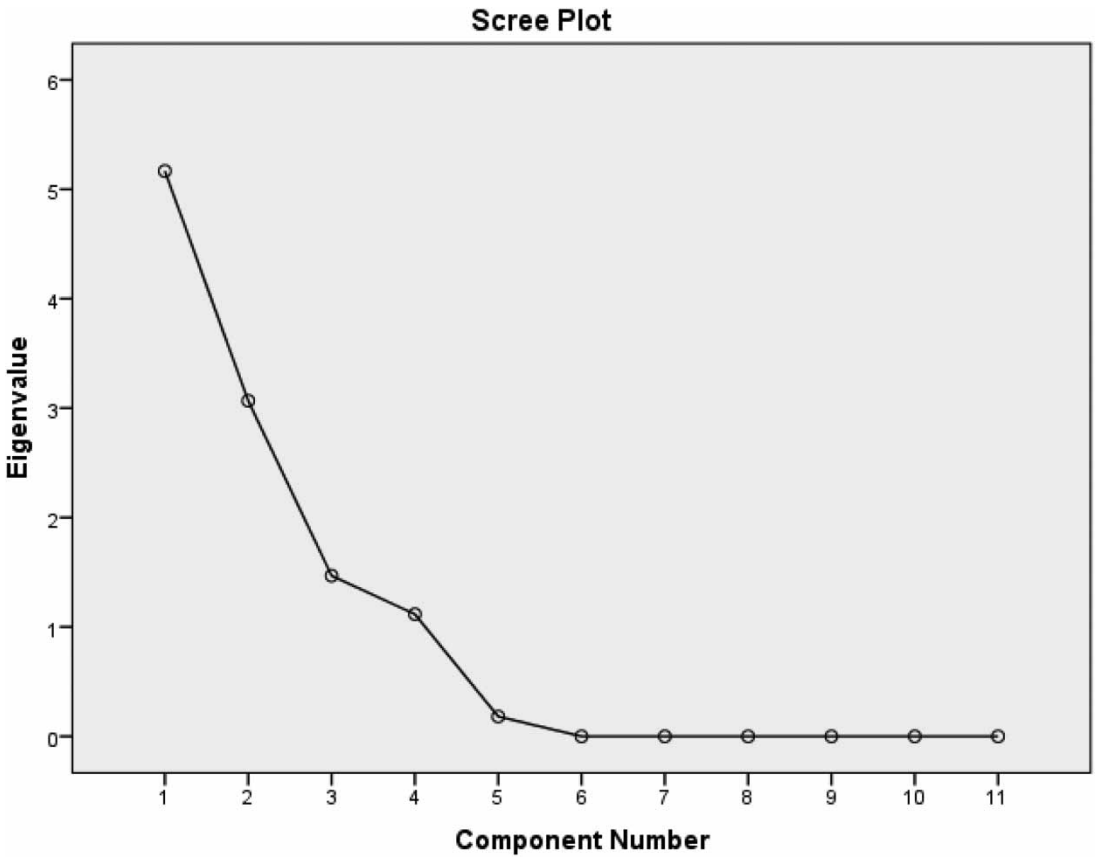

Figure 2 | Scree plot of factor loadings.

E.C., sodium, magnesium, and TDS marked factor 1, which explained 46.969% of the total variance. Factor 1 had a high positive loading for E.C. (0.993), sodium (0.848), magnesium (0.798), and TDS (0.749), respectively. On the other hand, Factor 1 had high negative loading on sulphur and carbonate: −0.961 and −0.734, respectively. High positive loadings indicated a strong linear correlation between the factor and parameters. Usage of fertilisers pesticides and herbicides can be marked as factor 1, obviously of anthropogenic origins from the agricultural land use. Factor 2, with higher positive loading of sulphates and calcium, explained 27.883% of the variance with a loading of 0.879 and 0.810. Factor 2 had a negative loading on pH; −0.996. Factor 3 accounted for 13.352% of the total variance and best represented by nitrates and partly calcium, 0.607 and 0.527, respectively. Groundwater of high TDS value encourages the mobilisation of compound contaminants such as carbonates, and nitrates. This single fact confirms the relationship between TDS and other compound contaminants. Leaching through downward washing of fertilisers through the overlying lateritic sand can increase the potassium of the groundwater and the process is evidenced in higher TDS values. Dissolved solids can produce hard water, which leaves deposits and films on fixtures, and on the insides of hot water pipes and boilers. Soaps and detergents do not produce as much lather with hard water as with soft water. As well as this, high amounts of dissolved solids can stain household fixtures, corrode pipes, and have a metallic taste. Factor 4 was responsible for 10.151% of total variance and was best represented by carbonates (0.440) and sodium (0.430). Groundwater of high sodium value is probably indicative of natural occurrence. This is an indication that groundwater with high levels of dissolved inorganic salts must have originated from water that has flowed through a region where the rocks have a high salt content (Amanambu 2015). Groundwater of high calcium value encourages

the higher dissolution of solids leading to hardness of water. The human body needs calcium for strong teeth and bones.

Spatial interpolation and groundwater modelling

Spatial modelling accuracy

Kriging is a geostatistical approach for interpolating a surface from a distributed collection of known points in order to forecast a continuous surface of values between specific places. Kriging weights are controlled using the Variogram model. The mathematical definition of a variogram is a measure of semi-variance as a function of distance.

$$\gamma(h) = \frac{1}{2N(h)} \sum_{i=1}^{N(h)} [z(x_i - z(x_i + h)]^2 \quad (1)$$

where $\gamma(h)$ is the semi-variance; $N(h)$ the number of pairs separated by distance or lag h; $z(x_i)$ the measured sample at point x_i; and $z\ (x_i + h)$ the measured sample at point $(x_i + h)$. Fitting a mathematical model to the experimental data determines the spatial organisation of the data. The mathematical models depict the structure of the spatial heterogeneity as well as the Kriging input parameters. The model was fit to the water quality parameters, which revealed spatial autocorrelation in their functional limits.

The experimental semi-variogram of data pairs was fitted using five models (Table 4). Nugget and sill parameters were computed by the Geostatistical Analyst tool for each model, and there was no basis to alter them (Setianto & Triandini 2013). The nugget is essentially the *Y*-intercept of the semi-variogram model, while sill is the semi-variogram value at which the model smoothens out (Munyati & Sinthumule 2021). However, the spherical model appeared to be the most consistent having yielded both the nugget and sill ratio, within the confines of this study.

The mean error (*ME*) indicates the probability of the predictions made by the Kriging method of being biased based on the possibility of an average as too high or too low. It reflects the average difference between the measured and the predicted values. It is expressed as

$$ME = \frac{\sum_{i=1}^{n} (\hat{Z}\ (S_i) - Z\ (S_i))}{n} \quad (2)$$

The root mean square error (*RMSE*) indicates how closely a model predicts the measured values and it is expressed mathematically as:

$$RMSE = \sqrt{\frac{\sum_{i=1}^{n} (\hat{Z}\ (S_i) - Z\ (S_i))^2}{n}} \quad (3)$$

The average standard error (*ASE*) presents the mean of prediction errors

$$ASE = \sqrt{\frac{\sum_{i=1}^{n} \hat{\sigma}^2\ (S_i)}{n}} \quad (4)$$

The root mean square error standardised (*RMSES*), indicates over or under estimation of the model predictions.

$$RMSES = \sqrt{\frac{\sum_{i=1}^{n} ((\hat{Z}\ (S_i) - Z\ (S_i)\ / \hat{\sigma}(S_i))^2}{n}} \quad (5)$$

where n is the sample size (number of data points), $z(S_i)$ is the measured value (number of individual parameters) at location S_i, $z(S_i)$ is the estimated value (predicted value of individual parameters) at location S_i, and $\sigma^2(S_i)$ is the

Table 4 | Comparative error of the semi-variogram models and parameters tested

Parameter	Model	N	Nugget	Sill
pH	Spherical	60	0.868	0.132
	Circular	60	0.879	0.102
	Stable	60	0.899	0.101
	Gaussian	60	0.923	0.077
	Exponential	60	0.864	0.136
E.C.	Spherical	60	0.969	0.052
	Circular	60	0.997	0.024
	Stable	60	1.007	0.015
	Gaussian	60	1.028	0.022
	Exponential	60	1.038	0.0
TDS	Spherical	60	0.965	0.052
	Circular	60	1.016	0
	Stable	60	1.001	0
	Gaussian	60	1.016	0
	Exponential	60	1.016	0
Ca	Spherical	60	0.550	0.465
	Circular	60	0.766	0.394
	Stable	60	0.704	0.312
	Gaussian	60	0.702	0.313
	Exponential	60	0.457	0.557
Mg	Spherical	60	0.957	0.065
	Circular	60	1.016	0.011
	Stable	60	1.010	0.012
	Gaussian	60	1.017	0.009
	Exponential	60	0.995	0
Na	Spherical	60	0.488	0.222
	Circular	60	0.494	0.223
	Stable	60	0.533	0.189
	Gaussian	60	0.551	0.189
	Exponential	60	0.447	0.278
Cl	Spherical	60	0.498	0.905
	Circular	60	0.554	0.872
	Stable	60	0.454	0.991
	Gaussian	60	0.608	0.759
	Exponential	60	0.166	1.275
HCO_3	Spherical	60	0.528	0.176
	Circular	60	0.549	0.154
	Stable	60	0.579	0.133
	Gaussian	60	0.559	0.153
	Exponential	60	0.476	0.230
K	Spherical	60	0.755	0.462
	Circular	60	0.777	0.466
	Stable	60	0.847	0.402
	Gaussian	60	0.840	0.410
	Exponential	60	0.625	0.598
SO_4	Spherical	60	0.797	0.527
	Circular	60	0.847	0.484
	Stable	60	0.943	0.392
	Gaussian	60	0.925	0.412
	Exponential	60	1.002	0.327
NO_3	Spherical	60	0.841	0.175
	Circular	60	1.016	0
	Stable	60	1.016	0
	Gaussian	60	1.016	0
	Exponential	60	1.016	0

Kriging variance for the *i*th data point (Munyati & Sinthumule 2021). If indication of the comparative suitability of a semi-variogram model could not be derived based on the combination of all three cross-validation statistics, ME and RMSES were prioritised because they indicated the extent to which the model interpolation predictions deviated or agreed from the measured values (Johnson *et al.* 2018; Elubid *et al.* 2019). The values of these four cross-validation techniques help to adequately understand and better explain the accuracy of the predicting model. The model posits that the closer the values of the ME and RMSES are to null (zero) and unity (one), respectively, the more accurate the model is and vice versa.

The cross-validation statistics criteria used ensured that the predictions are unbiased, this is indicated by: (1) an ME close to null (zero) (Gharbia *et al.* 2016), (2) estimates do not diverge significantly from the field observed values, indicated by a difference between the RMSE and ASE that is as small as possible (Nas & Berktay 2010), and (3) standard errors are precise, indicated by an RMSES prediction error close to unity (one) (Munyati & Sinthumule 2021).

Based on the cross-validation criteria to ensure unbiased predictions, the best model for the prediction of parameter concentration level was developed using a stable semi-variogram and true anisotropy. Table 5 presents the model accuracy measures as a result of the cross-validation matrix. The cross-validation matrix produced ME values that are close to zero ranging between −1.735 and 0.004; RMSES values that ranged between 0.821 and 1.134 (these values are close to 1, without approximation); and the least difference in the values of ASE and RMSE criss-crossing the entire data considered ranging between 0.058 and 33.078, to represent each parameter within the study. Co-Kriging surfaces were also constructed utilising covariate pairings and a stable, anisotropic semi-variogram. Cross-validation tests for parameter concentration found that the accuracy metrics (ME, RMSES, ASE, and RMSE) gave similar values across the sample points for each of the parameters.

Table 5 | Model accuracy metrics

Variables	ME	RMSES	ASE	RMSE	(ASE – RMSE)
pH	0.004	1.134	0.429	0.487	−0.058
E.C.	−0.797	0.907	326.67	323.96	2.71
TDS	−0.685	1.081	266.22	287.87	−21.65
HCO_3	−0.507	0.829	101.55	84.432	17.118
Ca	−0.246	0.821	25.579	27.577	−1.998
Mg	0.025	0.996	1.246	1.242	0.004
Na	−0.006	0.535	20.163	21.998	−1.835
NO_3	−0.209	0.899	6.836	7.378	0.821
Cl^-	−1.735	0.877	346.51	279.71	66.8
K	0.011	1.009	1.198	1.183	0.015
SO_4	−0.133	0.882	9.271	9.207	1.204

Furthermore, spatial correlations were quantified with the aid of the semi-variogram. In sum, the application of Kriging with semi-variogram models is proportional to the expected squared differences between the paired variables, i.e., the data values *(x)* and the distance lag, which separates different locations *(h)* (Gharbia *et al.* 2016). The spherical semi-variogram model being the most consistent was used for each water quality parameter. The Predictive performance of the fitted model had previously been evaluated using the cross-validation tests (Table 5). After the cross-validation process, maps of spatial estimates of parameters were generated to render a visual interpretation of the distribution of water quality parameters. As well as the best-fitted semi-variograms for the water quality parameters for the study area.

Geostatistical modelling

The normalcy of the investigated water quality parameters (pH, E.C., TDS, HCO_3, Ca, Mg, Na, NO^3, Cl^-, S, SO^4) was taken into account for the optimal performance of Kriging techniques. The ASE, RMSE and RMSES values were used to choose the best-fitting semi-variogram models (Table 4). Each of the Kriging algorithms, in addition

to providing projections, provides the Kriging variations, which measure the variability of the forecasts from the measured value. When RMSES is near unity (1), the model is deemed effective and produces the best accurate estimates. The Semi-variance analysis is a technique to assess the geographical dependency of the groundwater quality index (GWQI), which revealed that the estimated index was modelled using multiple semi-variogram models. The results of the selecting of the best-fitted variogram model show that spherical model was found as the most accurate model for water quality parameters. For all water quality parameter values, the exponential semi-variogram model is suited best (Figure 3(a)–3(k)).

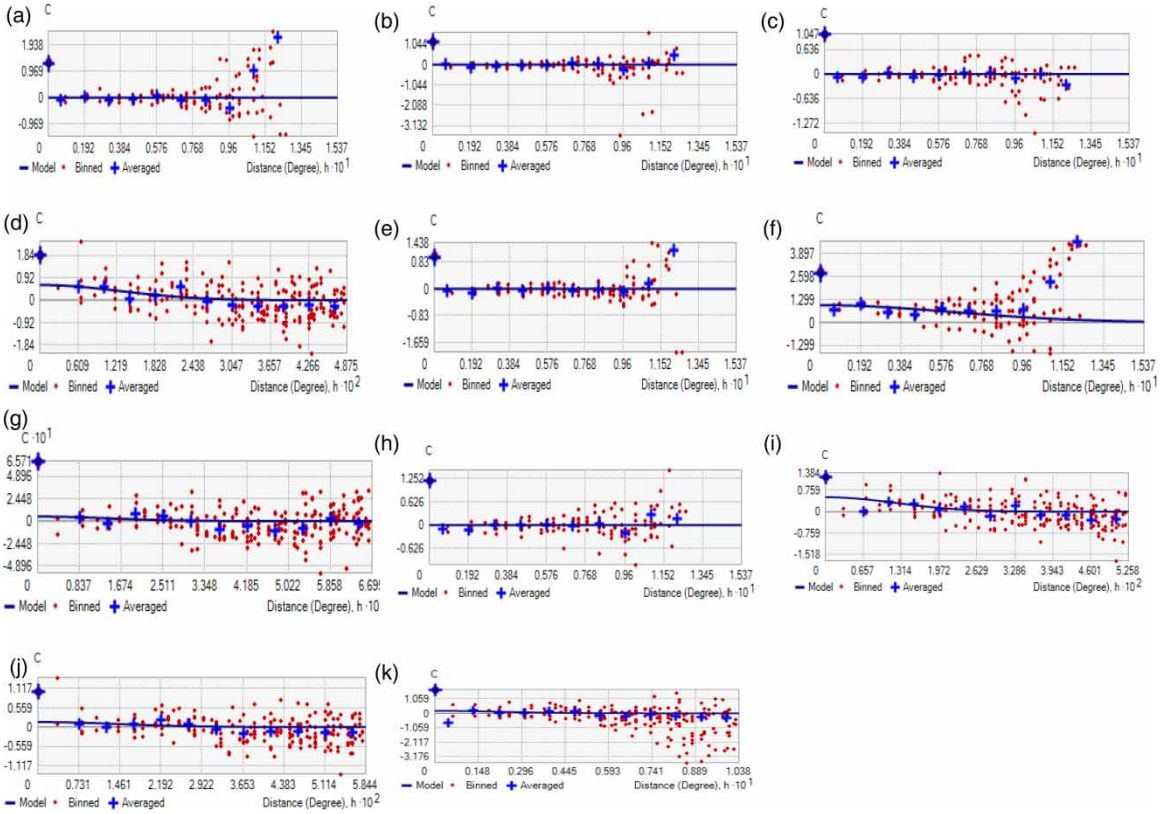

Figure 3 | (a)–(k) Best-fitted semi-variogram models for water quality parameters. (a) pH, (b) E.C., (c) TDS, (d) calcium, (e) magnesium, (f) sodium, (g) carbonate, (h) nitrates, (i) chloride, (j) potassium, and (k) sulphates.

Spatial prediction of concentration levels

A prediction/spatial variation map was generated to show the variation of pH over the study area (Figure 4(a)–4(k)). The coordinates of the sample points were used to aid in the depiction of the parameter over space. The map revealed that all the simulated pH levels were within the range +6.1 to +6.8 which were all in the slightly acidic range, and fall within permissible limits. TDS being a measure of materials dissolved in water, it is a measure of the combined content of all inorganic and organic substances contained in a liquid in molecular, ionised or micro-granular suspended form (Thomas 2021). The simulated TDS values as obtained from laboratory analysis ranged between 402.79 and 715.44 mg/l. The map revealed that lower levels of TDS are dispersed across the study area stretching from the centre region of the study area while higher values of TDS was predicted at upper central region (point 5), and the south-western area of the entire study area (points 58 and 59). The simulated E.C. values as obtained from laboratory analysis ranged between 726.95 and 1,046.57 μS/cm. The map revealed that mid-range values and lower levels of E.C. are dispersed across the study area stretching from the centre region of the study area while higher values of E.C. was predicted at upper central region (points 45 and 49), and the north-western area of the entire study area (points 22, 44, and 46). Calcium (Ca^{+}) was simulated following the values obtained from laboratory analysis and it ranged between 13.14 and 57.81 mg/l. The map revealed that higher concentration levels of calcium (Ca^{+}) are clustered towards the central region (points 25,

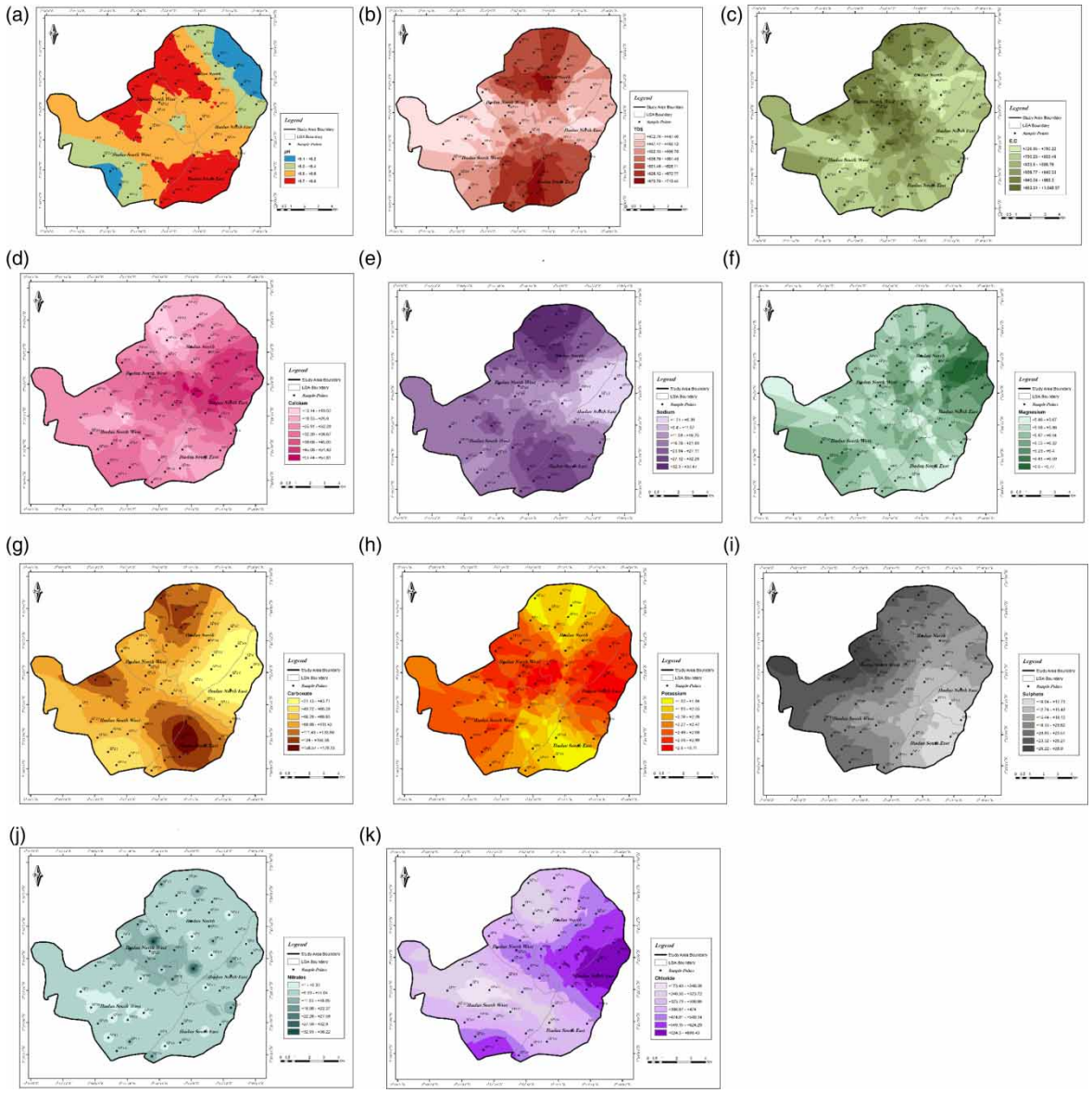

Figure 4 | (a)–(k) Optimal surface prediction for water quality parameters using Kriging showing local governments. (a) pH, (b) TDS, (c) E.C., (d) calcium, (e) sodium, (f) magnesium, (g) HCO_3, (h) potassium, (i) SO_4, (j) NO_3, and (k) Cl^-.

31, 34), while lower concentration values of calcium (Ca^+) was observed to be spread across the eastern stretch of the study area. Mid-range values were observed to be dispersed across the study area. Sodium (Na^+) values ranged between 1.21 and 37.47 mg/l. The map revealed that higher concentration levels of sodium (Na^+) can be found towards the northern end of the study area (points 29, 45, 49, 54, and 56) and the southwestern end of the study area (points 3, 52, 57, 58, and 59). Magnesium (Mg^{2+}) values ranged between 5.49 and 6.77 mg/l. Higher concentration levels of magnesium (Mg^{2+}) are clustered towards north-east of the study area (points 6, 12, and 30) while lower concentration and mid-range values were observed to be dispersed across the study area. Carbonates (HCO_3^-) values ranged between 21.13 and 179.13 mg/l. Very high concentration levels of carbonates (HCO_3^-) are clustered towards south-eastern end of the study area (points 58 and 59), as well as at the north-central end (points 45, 49, 54, and 56) with high concentration values. Lower concentration and mid-range values were observed to be discrete across the study area. Potassium (K^+) ranged between 1.62 and 3.11. Very high concentration levels of potassium (K^+) are clustered towards north-east of the study area (points 6, 13, 18, 25, 27, and 30), as well as at the north-west end (points 1, 4, 22, 24, 32, 44, and 46) with high concentration values as well. Mid-range values and lower concentration were observed to be

spread out across the study area. Sulphate (SO_4^{2-}) values ranged between 10.04 and 28.9 mg/l. The map revealed that higher concentration levels of sulphate (SO_4^{2-}) was recorded at sample points 2, 4, 41 and 42, and 15 towards the western end of the study area; and at sample points 45 and 29 in the north end of the study area. While lower concentration values of sulphate (SO_4^{2-}) was scattered around the central west and southern section of the study area. Mid-range values were observed to be dispersed across the study area. The nitrates (NO_3^-) values ranged between 1.0 and 38.22 mg/l. Higher concentration levels of nitrates (NO_3^-) was recorded at sample points 1 and 31 only. Mid-range concentration values and lower concentration values of nitrates (NO_3^-) are dispersed across the study area. The chloride (Cl^-) values ranged between 173.43 and 699.43 mg/l. Higher concentration levels of chloride (Cl^-) was recorded at sample points 21, 25 and 31 only. Mid-range concentration values and Lower concentration values of chloride (Cl^-) are dispersed across the study area.

Groundwater suitability

The GWQI was used to estimate the suitability of the water for consumption. This index provides an unbiased measure of water quality considering all the measured parameters for each water sample. The GWQI is a recently adopted method for revealing the quality of groundwater at a glance. The Water Quality Index (WQI) computations for each sampling location in the current study involved three successive steps (Li *et al.* 2011). The first step was 'assigning of weight'. Each of the parameters except were assigned weights (W_i), according to their relative importance in the overall drinking water quality. The most significant parameters were given a weight of 5 and the least significant a weight of 1 (Mahmud *et al.* 2020).

The second step will be the calculation of relative weights for each water quality feature. The relative weight (W_i) was computed using Equation (5) as pointed out by Mahmud *et al.* (2020).

$$W_i = \frac{w_i}{\sum_{i=1}^{n} w_i} \tag{6}$$

where W_i is the relative weight, w_i is the weight of each parameter, and n is the number of parameters.

The third step was the computation of the quality rating scale. The quality rating scale (q_i) for each parameter was calculated using Equation (6) (Iwar *et al.* 2021):

$$q_i = \frac{C_i}{S_i} * 100 \tag{7}$$

where q_i is the quality rating, C_i is the concentration of each chemical parameter in each water sample in mg/l, except pH, and S_i is the World Health Organisation (WHO) standard for each chemical parameter.

Table 6 | Relative weights of parameters in the study area

Parameters	WHO standard	Unit weight	W_i	q_i	$W_i q_i$
pH	7.5	0.1333	0.456360525	86.66666667	39.55125
EC	400	0.0025	0.00855676	223.389625	1.911491
TDS	500	0.0020	0.006845408	107.37534	0.735028
Sodium	200	0.0050	0.01711352	15.98115	0.273494
Magnesium	50	0.0200	0.068454079	12.0374	0.824009
Calcium	100	0.0100	0.034227039	4.7102	0.161216
Chloride	250	0.0040	0.013690816	178.00248	2.436999
Potassium	12	0.0833	0.285225328	18.79166667	5.359859
Carbonates	125	0.0080	0.027381631	202.40064	5.54206
Sulphates	250	0.0040	0.013690816	7.86988	0.107745
Nitrates	50	0.0200	0.068454079	19.318	1.322396
Sum			1		58.22554

Finally, the W_i and q_i were used to compute the SI_i for each chemical parameter (Equation (7)), and then the WQI was calculated using Equation (8).

$$SI_i = W_i * q_i \tag{8}$$

$$WQI = \sum_{i=1}^{n} SI_i \tag{9}$$

where SI_i is the sub-index of each parameter, q_i is the rating based on the concentration of each parameter, and n is the number of parameters'. The computed GWQI values for each location were categorised, and detailed computations for the GWQI for each location and parameter was provided (Table 6) (Al-Omran *et al.* 2015; Bashir *et al.* 2020).

The overall weight of the GWQI shows that the water in the study area falls within the good water range (Table 7), of the groundwater classification according to Sahu & Sikdar (2008) and Belkhiri *et al.* (2020).

Table 7 | Classification of groundwater based on the GWQI

Range	Type of water
<50	Excellent
50–100.1	Good water
100–200.1	Poor water
200–300.1	Very poor water
>300	Water unsuitable for drinking purposes

CONCLUSION

Geostatistical analysis techniques, such as Kriging, are considered to be useful techniques for the monitoring, evaluation and management of groundwater resources. This study uses Kriging geostatistical technique and the GWQI to map the spatial variability of groundwater quality parameters. The groundwater quality analyses were done for Ibadan Metropolitan area using a GIS-based geostatistical algorithm. Factor analysis was employed to understand the influence of prevalent human activities on each parameter.

This study found a significant correlation between anthropogenic factors and concentration levels of water quality parameters in groundwater wells. This study on the overall provided a local government level concentration prediction mapping in the Ibadan metropolis. The study generated prediction models that estimated the presence of different parameters in groundwater where direct measurements were not possible. The results of this study will be useful for residents or housing developers installing new water wells to avoid areas that are known, or predicted, to contain concentrations of parameters greater than the established WHO and USEPA secondary water quality criteria.

DATA AVAILABILITY STATEMENT

Data cannot be made publicly available; readers should contact the corresponding author for details.

CONFLICT OF INTEREST

The authors declare there is no conflict.

REFERENCES

Adimalla, N., Venkatayogi, S. & Das, S. V. G. 2019 Assessment of fluoride contamination and distribution: a case study from a rural part of Andhra Pradesh, India. *Applied Water Science* **9**(4), 1–15. https://doi.org/10.1007/s13201-019-0968-y.

Ahmadi, S., Jahanshahi, R., Moeini, V. & Mali, S. 2018 Assessment of hydrochemistry and heavy metals pollution in the groundwater of Ardestan mineral exploration area, Iran. *Environmental Earth Sciences* **77**(5), 1–13. https://doi.org/10.1007/s12665-018-7393-7.

Ali, S. A. & Ahmad, A. 2020 Analysing water-borne diseases susceptibility in Kolkata Municipal Corporation using WQI and GIS based Kriging interpolation. *GeoJournal* **85**(4), 1151–1174. https://doi.org/10.1007/s10708-019-10015-3.

Al-Omran, A., Al-Barakah, F., Altuquq, A., Aly, A. & Nadeem, M. 2015 Drinking water quality assessment and water quality index of Riyadh, Saudi Arabia. *Water Quality Research Journal of Canada* **50**(3), 287–296. https://doi.org/10.2166/wqrjc.2015.039.

Amanambu, A. C. 2015 Geogenic contamination: hydrogeochemical processes and relationships in shallow aquifers of Ibadan, South-West Nigeria. *Bulletin of Geography. Physical Geography Series* **9**(1), 5–20. https://doi.org/10.1515/bgeo-2015-0011.

Aragaw, T. T. & Gnanachandrasamy, G. 2021 Evaluation of groundwater quality for drinking and irrigation purposes using GIS-based water quality index in urban area of Abaya-Chemo sub-basin of Great Rift Valley, Ethiopia. *Applied Water Science* **11**(9), 1–20. https://doi.org/10.1007/s13201-021-01482-6.

Bashir, N., Saeed, R., Afzaal, M., Ahmad, A., Muhammad, N., Iqbal, J., Khan, A., Maqbool, Y. & Hameed, S. 2020 Water quality assessment of lower Jhelum canal in Pakistan by using geographic information system (GIS). *Groundwater for Sustainable Development* **10**(February). https://doi.org/10.1016/j.gsd.2020.100357.

Belkhiri, L., Tiri, A. & Mouni, L. 2020 Spatial distribution of the groundwater quality using kriging and co-kriging interpolations. *Groundwater for Sustainable Development* **11**(February), 100473. https://doi.org/10.1016/j.gsd.2020.100473.

Boudibi, S., Sakaa, B. & Zapata-Sierra, A. J. 2019 Groundwater quality assessment using Gis, Ordinary Kriging and WQI in an arid area. *PONTE International Scientific Researchs Journal* **75**(12), 204–226. https://doi.org/10.21506/j.ponte.2019.12.14.

Bouteraa, O., Mebarki, A., Bouaicha, F., Nouaceur, Z. & Laignel, B. 2019 Groundwater quality assessment using multivariate analysis, geostatistical modeling, and water quality index (WQI): a case of study in the Boumerzoug-El Khroub valley of Northeast Algeria. *Acta Geochimica* **38**(6), 796–814. https://doi.org/10.1007/s11631-019-00329-x.

Busico, G., Kazakis, N., Cuoco, E., Colombani, N., Tedesco, D., Voudouris, K. & Mastrocicco, M. 2020 A novel hybrid method of specific vulnerability to anthropogenic pollution using multivariate statistical and regression analyses. *Water Research* **171**, 115386. https://doi.org/10.1016/j.watres.2019.115386.

Dar, F. A., Ganai, J. A., Ahmed, S. & Satyanarayanan, M. 2017 Groundwater trace element chemistry of the karstified limestone of Andhra Pradesh, India. *Environmental Earth Sciences* **76**(20). https://doi.org/10.1007/s12665-017-6972-3.

Díaz-Alcaide, S. & Martínez-Santos, P. 2019 Review: advances in groundwater potential mapping. *Hydrogeology Journal* **27**(7), 2307–2324. https://doi.org/10.1007/s10040-019-02001-3.

Dube, T., Shoko, C., Sibanda, M., Baloyi, M. M., Molekoa, M., Nkuna, D., Rafapa, B. & Rampheri, B. M. 2020 Spatial modelling of groundwater quality across a land use and land cover gradient in Limpopo Province, South Africa. *Physics and Chemistry of the Earth* **115**(November), 102820. https://doi.org/10.1016/j.pce.2019.102820.

Egbinola, C. N. & Amanambu, A. C. 2014 Groundwater contamination in Ibadan, South-West Nigeria. *SpringerPlus* **3**(1), 2–7. https://doi.org/10.1186/2193-1801-3-448.

Elubid, B. A., Huag, T., Ahmed, E. H., Zhao, J., Elhag, K. M., Abbass, W. & Babiker, M. M. 2019 Geospatial distributions of groundwater quality in Gedaref state using geographic information system (GIS) and drinking water quality index (DWQI). *International Journal of Environmental Research and Public Health* **16**(5), 1–20. https://doi.org/10.3390/ijerph16050731.

Fallah, B., Richter, A., Ng, K. T. W. & Salama, A. 2019 Effects of groundwater metal contaminant spatial distribution on overlaying kriged maps. *Environmental Science and Pollution Research* **26**(22), 22945–22957. https://doi.org/10.1007/s11356-019-05541-z.

Gharbia, A. S., Gharbia, S. S., Abushbak, T., Wafi, H., Aish, A., Zelenakova, M. & Pilla, F. 2016 Groundwater quality evaluation using GIS based geostatistical algorithms. *Journal of Geoscience and Environment Protection* **04**(02), 89–103. https://doi.org/10.4236/gep.2016.42011.

Gu, X., Xiao, Y., Yin, S., Hao, Q., Liu, H., Hao, Z., Meng, G., Pei, Q. & Yan, H. 2018 Hydrogeochemical characterization and quality assessment of groundwater in a long-term reclaimed water irrigation Area, North China Plain. *Water (Switzerland)* **10**(9), 1–16. https://doi.org/10.3390/w10091209.

He, S. & Wu, J. 2019 Relationships of groundwater quality and associated health risks with land use/land cover patterns: a case study in a loess area, Northwest China. *Human and Ecological Risk Assessment* **25**(1–2), 354–373. https://doi.org/10.1080/10807039.2019.1570463.

Iwar, R. T., Ogedengbe, K., Katibi, K. K. & Jabbo, J. N. 2021 Fluoride levels in deep aquifers of Makurdi, North-central, Nigeria: an appraisal based on multivariate statistics and human health risk analysis. *Environmental Monitoring and Assessment* **193**(8), 1–15. https://doi.org/10.1007/s10661-021-09230-8.

Jia, Y., Xi, B., Jiang, Y., Guo, H., Yang, Y., Lian, X. & Han, S. 2018 Distribution, formation and human-induced evolution of geogenic contaminated groundwater in China: A review. In: *Science of the Total Environment*, Vol. 643. Elsevier B.V, pp. 967–993. https://doi.org/10.1016/j.scitotenv.2018.06.201

Jiang, W., Wang, G., Sheng, Y., Shi, Z. & Zhang, H. 2019 Isotopes in groundwater (2 H, 18 O, 14 C) revealed the climate and groundwater recharge in the Northern China. *Science of the Total Environment* **666**, 298–307. https://doi.org/10.1016/j.scitotenv.2019.02.245.

Johnson, C. D., Nandi, A., Joyner, T. A. & Luffman, I. 2018 Iron and manganese in groundwater: using kriging and GIS to locate high concentrations in Buncombe County, North Carolina. *Groundwater* **56**(1), 87–95. https://doi.org/10.1111/gwat.12560.

Kaiser, H. F. 1960 The application of electronic computers to factor analysis. educational and psychological measurement. *Educational and Psychological Measurement* **20**(1), 141–151. https://doi.org/10.1177/001316446002000116.

Li, M., Zhu, X., Zhu, F., Ren, G., Cao, G. & Song, L. 2011 Application of modified zeolite for ammonium removal from drinking water. *Desalination* **271**(1–3), 295–300. https://doi.org/10.1016/j.desal.2010.12.047.

Li, P., He, X. & Guo, W. 2019 Spatial groundwater quality and potential health risks due to nitrate ingestion through drinking water: a case study in Yan'an City on the Loess Plateau of northwest China. *Human and Ecological Risk Assessment* **25**(1–2), 11–31. https://doi.org/10.1080/10807039.2018.1553612.

Mahmud, A., Sikder, S. & Joardar, J. C. 2020 Assessment of groundwater quality in Khulna city of Bangladesh in terms of water quality index for drinking purpose. *Applied Water Science* **10**(11). https://doi.org/10.1007/s13201-020-01314-z.

Marghade, D., Malpe, D. B. & Subba Rao, N. 2019 Applications of geochemical and multivariate statistical approaches for the evaluation of groundwater quality and human health risks in a semi-arid region of eastern Maharashtra, India. *Environmental Geochemistry and Health* **43**(2), 683–703. https://doi.org/10.1007/s10653-019-00478-1.

Munyati, C. & Sinthumule, N. I. 2021 Comparative suitability of ordinary kriging and Inverse Distance Weighted interpolation for indicating intactness gradients on threatened savannah woodland and forest stands. *Environmental and Sustainability Indicators* **12**, 100151. https://doi.org/10.1016/j.indic.2021.100151.

Murphy, H. M., Prioleau, M. D., Borchardt, M. A. & Hynds, P. D. 2017 Review: epidemiological evidence of groundwater contribution to global enteric disease, 1948–2015. *Hydrogeology Journal* **25**(4), 981–1001. https://doi.org/10.1007/s10040-017-1543-y.

Narany, T. S., Ramli, M. F., Aris, A. Z., Sulaiman, W. N. A. & Fakharian, K. 2014 Spatial assessment of groundwater quality monitoring wells using indicator kriging and risk mapping, Amol-Babol Plain, Iran. *Water (Switzerland)* **6**(1), 68–85. https://doi.org/10.3390/w6010068.

Nas, B. & Berktay, A. 2010 Groundwater quality mapping in urban groundwater using GIS. *Environmental Monitoring and Assessment* **160**(1–4), 215–227. https://doi.org/10.1007/s10661-008-0689-4.

Obaid, A. N. & Mohammed, M. J. 2020 A comparison of topological Kriging and area to point kriging for irregular district area in Iraq. *Journal of Mechanics of Continua and Mathematical Sciences* **15**(4). https://doi.org/10.26782/jmcms.2020.04.00009.

Pazand, K., Khosravi, D., Ghaderi, M. R. & Rezvanianzadeh, M. R. 2018 Hydrogeochemistry and lead contamination of groundwater in the north part of Esfahan province, Iran. *Journal of Water and Health* **16**(4), 622–634. https://doi.org/10.2166/wh.2018.034.

Rata, M., Douaoui, A., Larid, M. & Daouik, A. 2018 Spatial analysis of annual rainfall using ordinary kriging techniques and lognormal kriging in the Cheliff watershed. Algeria. *Journal of Environmental Sciences* **1**(1), 1–9. Available from: www.nessapublishers.com

Sahu, P. & Sikdar, P. K. 2008 Hydrochemical framework of the aquifer in and around East Kolkata Wetlands, West Bengal, India. *Environmental Geology* **55**(4), 823–835. https://doi.org/10.1007/s00254-007-1034-x.

Saito, T., Spadini, L., Saito, H., Martins, J. M. F., Oxarango, L., Takemura, T., Hamamoto, S., Moldrup, P., Kawamoto, K. & Komatsu, T. 2020 Characterization and comparison of groundwater quality and redox conditions in the Arakawa Lowland and Musashino Upland, southern Kanto Plain of the Tokyo Metropolitan area, Japan. *Science of the Total Environment* **722**, 137783. https://doi.org/10.1016/j.scitotenv.2020.137783.

Selmane, T., Mostefa, D., Djerbouai, S., Djemiat, D. & Lemouari, N. 2022 Groundwater quality assessment using water quality indices and GIS technique with kriging interpolation in Maadher plain of Hodna, northern Algeria. *Research Square* 0–19. https://doi.org/10.21203/rs.3.rs-1647543/v1.

Setianto, A. & Triandini, T. 2013 Comparison of Kriging and Inverse Distance Weighted (IDW) interpolation methods in lineament extraction and analysis. *Journal of Applied Geology* **5**(1), 21–29. https://doi.org/10.22146/jag.7204.

Thomas, E. O. 2021 Effect of temperature on D.O and T.D.S: a measure of ground and surface water interaction. *Water Science* **35**(1), 11–21. https://doi.org/10.1080/11104929.2020.1860276.

Venkatramanan, S., Chung, S. Y., Kim, T. H., Kim, B. W. & Selvam, S. 2016 Geostatistical techniques to evaluate groundwater contamination and its sources in Miryang City, Korea. *Environmental Earth Sciences* **75**(11). https://doi.org/10.1007/s12665-016-5813-0.

Wang, Z., Guo, H., Xiu, W., Wang, J. & Shen, M. 2018 High arsenic groundwater in the Guide basin, northwestern China: distribution and genesis mechanisms. *Science of the Total Environment* **640–641**, 194–206. https://doi.org/10.1016/j.scitotenv.2018.05.255.

Wang, Y., Li, J., Ma, T., Xie, X., Deng, Y. & Gan, Y. 2021 Genesis of geogenic contaminated groundwater: As, F and I. In: *Critical Reviews in Environmental Science and Technology*, Vol. 51, 24. Taylor & Francis, pp. 2895–2933. https://doi.org/10.1080/10643389.2020.1807452.

Xiao, Y., Shao, J., Frape, S. K., Cui, Y., Dang, X., Wang, S. & Ji, Y. 2018 Groundwater origin, flow regime and geochemical evolution in arid endorheic watersheds: a case study from the Qaidam Basin, Northwestern China. *Hydrology and Earth System Sciences* **22**(8), 4381–4400. https://doi.org/10.5194/hess-22-4381-2018.

First received 1 November 2022; accepted in revised form 11 February 2023. Available online 22 February 2023